Dosimetry calculations of gastric cancer treatment during pencil beam scanning proton therapy

S. Sadrzadeh and M. Tajik*

School of Physics, Damghan University, P.O. Box 36716-41167, Damghan, Iran

ABSTRACT

► *Original article*

Background: In this study, Monte Carlo simulations were performed to estimate the dose of proton therapy to involved and uninvolved organs in gastric cancer. **Materials and Methods:** The dose received by involved and uninvolved organs during gastric treatment was simulated during pencil beam scanning proton therapy using the MIRD-UF phantom and the MCNPX code. In this modeling, the appropriate energy range for tumor treatment in the gastric tissue of an adult male MIRD-UF phantom with monoenergetic proton beams was calculated. The dose secondary charged particles, neutrons and photons in the tumor and vital organs were evaluated. **Results:** The results showed that, depending on the size of the tumor, the appropriate and optimal range of proton energy to cover the tumor is 67 - 81.5 MeV. The distribution of energy deposition, total primary dose, and the ratio of neutron equivalent dose to absorbed therapeutic dose (H/D) were calculated for the tumor and 12 vital organs. The ratio between the total received dose of the healthy gastric tissue and the delivered dose of the tumor was about 0.0046. The average photon equivalent dose was about 0.9% of the neutrons. The highest H/D ratios for normal stomach, spleen, pancreas, and left kidney tissue were 0.167 mSv/Gy, 0.0362 mSv/Gy, 0.0231 mSv/Gy and 0.0143 mSv/Gy, respectively. **Conclusion:** In the study, a small gastric tumor in an adult male phantom was irradiated with high-energy protons. Proton therapy delivered the highest possible dose to the tumor, while the healthy organs received a low dose.

INTRODUCTION

More than 50% of patients with local malignant tumors are treated with radiotherapy. This shows the need to find methods with minimal side effects [1]. Proton therapy, based on an intelligent manipulation of the specific dose-depth characteristic of this beam, the "Bragg Peak", is highly regarded in today's clinical world [2].

In ideal radiotherapy, the aim is to protect as much healthy tissue as possible from the radiation, while the tumor receives the maximum dose. Protons are superior to photons in the treatment of local tumors due to their low lateral scattering, limited range in tissue and constant relative biological effect. In general, proton therapy is suitable for the treatment of local tumors, and its benefits have been confirmed in the treatment of various cancers, including ocular melanoma, chordoma, chondrosarcoma, and liver cancer [3-7]. Proton technologies have made significant advances in medical programs since their introduction. Until recently, only passive dispersion methods were used, but active scanning has also been utilized [8]. Since the beams extracted from the accelerator have a single energy, the passive dispersion method uses a scattering foil, absorber, and filters to broaden the Bragg peak and achieve better tumor coverage [9].

The spot scanning method is a new method of proton irradiation in which a small volume is selected within the patient and the spots are irradiated one after the other by adjusting the energy of the beam. This method can reduce the unwanted dose to the healthy tissue around the tumor. It should be noted that the choice of treatment method depends on the location and size of the target [10]. Some researchers have confirmed the use of proton therapy in the treatment of gastric cancer [10-15].

Only a few clinical studies have been conducted on the use of proton therapy in the treatment of gastric tumors. Case reports from the College of Tsukuba from the last 30 years are the only published evidence. Koyama et al. reported the case of a 72-year-old man with advanced gastric cancer who was inoperable due to severe emphysema. Since surgery was not an option, chemotherapy with proton therapy up to a dose of 61 Gy was used as treatment. As a result of this treatment method, the tumor regressed and became necrotic, while the normal tissue structure around the tumor was healthy [14].

In 1991, Shiba *et al.* reported the treatment of two men aged 85 and 70 years with early inoperable gastric cancer with proton therapy. The patients received doses of 83-86 Gy, and subsequent endoscopy showed that the gastric ulcer was stable and tumor-free. Since then, no further clinical data

have been reported and no trials are currently ongoing [16].

As radiotherapy requires planning before treatment and patients cannot be used as test subjects, a computer simulation is used. Monte Carlo simulation allows the test conditions to be precisely defined. The Monte Carlo code MCNPX can track protons under clinical conditions and in volume-based phantoms and is used for radiotherapy simulation.

Studies have shown that proton therapy using the pencil beam scanning method reduces the secondary neutron dose by a factor of about ten compared to the passive scattering method [17-21]. The scanned proton beams can reduce the radiation received by vital organs through precise dose distribution. However, the radiation received by healthy body tissue can cause side effects.

As already mentioned, there are only a few clinical reports on the use of proton therapy in the treatment of gastric cancer. However, no theoretical studies have been conducted to estimate the dose of secondary particles to both involved and non-involved organs. This lack of research leaves out a crucial aspect when it comes to understanding the full extent and potential benefits of proton therapy for patients with gastric cancer.

The aim of this study was to simulate proton therapy for gastric tumors in order to estimate the dose received by the involved and non-involved organs. In this study, Monte Carlo simulations were performed for the dosimetry of involved and non-involved organs in gastric cancer during pencil beam proton scan treatment. Computer modeling of gastric irradiation was performed using a MIRD-UF phantom and the MCNPX code. Scanned proton beams can reduce the radiation absorbed by vital organs through accurate dose distribution. However, radiation absorbed by healthy body tissue can cause side effects.

MATERIALS AND METHODS

Most gastric tumors are adenocarcinomas (90-95%) [21]. A tumor of this type was formed in the stomach wall of an adult male MIRD-UF phantom. Primary gastric cancer tumors < 3 cm are classified as small tumors [22]. Therefore, small tumors in the shape of an elliptical cylinder (thickness: 0.4 cm, large diameter (3 cm), small diameter (1.5 cm), and about 3.6 cm below the skin surface) were considered. The composition of materials and the percentage of elements in the adenocarcinoma tumor tissue is as follows: Potassium (K) - 0.36%, Sulfur (S) - 0.54%, Phosphorus (P) - 0.36%, Chlorine (Cl) - 0.36%, Sodium (Na) - 0.18%, Oxygen (O) - 56.9%, Nitrogen (N) - 4.5%, Carbon (C) - 26.9%, and Hydrogen (H) - 9.9%. The density of the

adenocarcinoma tumor tissue is 1.04 g/cm^3 [24]. According to figure 1, the depth of this tumor along the y-axis ranges from -4.75 to -3.25. In this study, a simple pencil beam, which is the result of the pencil scanner system, was considered. The proton beam emits monoenergetic proton beams along the y-axis.
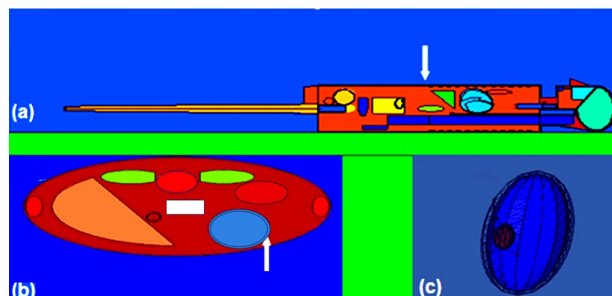
Figure 1. MIRD-UF phantom, irradiated with a pencil beam **a)** in the YZ plane, **b)** from the cross-sectional area inside the phantom in the XY plane, **c)** the gastric organ and the tumor in its wall separately and three-dimensionally.

Monte Carlo simulation

The simulation studies were performed with the MCNPX code version 2.6, Los Alamos, NM, USA. Using the MCNPX code [24], the geometry of the phantom limb, as shown in figure 1, together with its components, was exposed to proton irradiation at a specified energy.

The absorbed doses of protons, electrons, and positrons were calculated using tally F6. The absorbed dose obtained was expressed in terms of absorption energy per mass (MeV/g), which was multiplied by 1.602×10^{-10} to convert it into a unit (Gy/s). The energy deposition for the positron and electron produced by the interaction of a proton with an atom and a nucleus was calculated using the FT card ELC and the electron physics card. The FMn card was used to multiply the output by a fixed number to convert the unit of absorbed dose from (MeV/g) to (Gy/s).

Dose equivalent is generally used for neutrons with different relative biological effects (RBE) over a range of energies [25]. The doses of transported neutrons and photons were calculated using the F4 tally card, and the dose equivalent was calculated using a dose function (DF) card. The flux to dose conversion factors were based on the ANSI/ANS - 6.1.1-1977 report [26]. The dose equivalent obtained is expressed in Sv/h. To convert this unit to mSv/s, multiply by 2.778×10^{-1}. The FM card gives the unit of output in mSv/s. Another conventional measure typically used to calculate the secondary dose is the ratio of the neutron dose equivalent to the absorbed therapeutic dose (H/D). Where H is the neutron equivalent dose and D is the therapeutic absorbed or proton dose delivered to the tumor volume [28].

Using mesh tally card, we calculated various values such as flux, energy deposition, etc. in a meshed manner in each part of the geometry of the

problem. In this study, energy deposition in MeV/cm³ will be calculated in different organs of the body. In the input file of the MCNP code, the number of particle shifts (NPS card) is set to 10×10⁷. The maximum simulation error was about 1%. The data obtained from the simulation results were plotted using Origin software version 2024 (Learning Edition) [29].

The construction of the Spread-Out Bragg Peak (SOBP)

To determine the appropriate energy, range to completely cover the tumor volume, the energy of the beam was gradually increased. Since the Bragg peaks alone are narrow and not suitable to cover every target, they should be wide and form a SOBP. For this purpose, the number of peaks required and the weight of each Bragg peak involved in the construction of the SOBP were calculated. In this way, a uniform and maximum dose is delivered to the tumor. The three processes of stopping, scattering and nuclear interaction determine the shape of the Bragg peak (2). In this work, according to the average standard deviation of these peaks, which is about 1 mm, a distance between neighboring peaks of 1 mm was assumed to avoid overlapping of the peaks and to obtain a SOBP without waves. Therefore, to cover the tumor as much as possible, 16 peaks were included to generate a Spread-Out Bragg Peak.

The matrix method is a numerical method for calculating the weighting coefficients of Bragg peaks [29]. For this purpose, the desired geometry must first be deeply meshed by dividing the geometry of the problem in the XY plane into voxels with a size of 1 mm using a rectangular mesh. The energy deposition in each voxel was calculated using a tally mesh. In the next step, the data corresponding to each peak was listed in columns. In this case, an m×n matrix was created, where n is the number of desired peaks and m is the number of voxels generated. The maximum dose was determined in each column. The rows corresponding to these maxima should be placed one below the other so that they are on the major diameter of an n×n matrix. For example, the final matrix is 16 ×16.

The inverse of this n×n matrix is multiplied by an n×1 matrix, all corresponding to the maximum dose value to which the flat part of the SOBP should be normalized. Finally, the resulting n×1 matrix and its arrays correspond to the weights of the assumed peak values. Table 1 lists the weights of each energy in the formation of the SOBP. The weight of each peak indicates its contribution to the formation of the spread Bragg peak. In other words, these weights indicate the radiation time of each beam at a given energy. To obtain the optimal peak, the corresponding Bragg peaks must be multiplied by the obtained coefficients. Then the data for all peaks in each volume were summed to obtain the overall shape of the SOBP. The specifications of the adjusted SOBP based on the beam parameters can be found in ICRU Report No. 78 [30].

Table 1. The optimized weighting factors for the creation of SOBP.

| Energy (MeV)	Weighting factor	Energy (MeV)	Weighting factor
74	0.06818	81.5	1
73	0.05991	80.5	0.26636
72	0.04713	79.5	0.26406
71	0.04507	78.5	0.10988
70	0.03107	77.8	0.14921
69	0.03413	76.8	0.09106
68	0.01966	76	0.08983
67	0.03489	75	0.08187

Statistical analysis

Statistical analyses were performed using Origin software version OriginPro 2024 (Learning Edition) (Origin Lab Corporation, Northampton, MA, USA). The Origin software is used to draw and analyze numerical the output of mesh tally, F6 and F4 cards of MCNPX code. Based on the data from the output of the MCNP code cards, the changes in the distribution of energy deposition and dose, proton, neutron, electron and photon particles in the involved and non-involved organs were qualitatively plotted in 3D and 2D using Origin software. Due to the Origin software's powerful ability to analyze numerical and statistical data, a quantitative comparison was made between the deposited energy and dose for proton particles and secondary particles generated in the tumor and other organs.

RESULTS

The simulation results show that the appropriate range of proton energy to cover the tumor is ~ 67–81.5 MeV. The Bragg peaks associated with the calculation are shown in figure 2. In this figure, the energy deposition per unit volume is plotted against the penetration depth from the body surface for the incident proton beam in the above-mentioned energy range. The penetration depth of the beam into the tissue depends directly on the energy of the incident beam. The higher the energy of the proton beam, the deeper it penetrates. The appropriate energy range for the treatment of each tumor depends on the thickness of the tumor exposed to the beam. Therefore, tumor dimensions must be accurately measured using imaging techniques prior to treatment. Based on the data in figure 2, the changes in the penetration force of the particles as a function of proton energy are shown in figure 3. Fitting a curve to the data in figure 3 shows that the relationship between the initial energy of the proton and the range in the material medium is given by equation 1:

$$R = \alpha + \beta E^p \qquad (1)$$
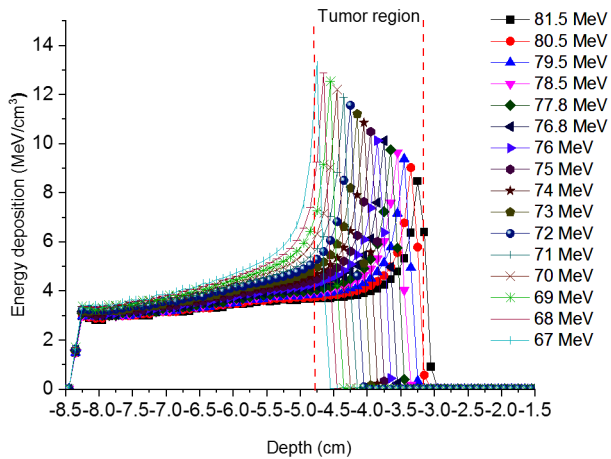
Figure 2. Energy deposition profiles in the stomach of the MIRD-UF phantom for protons with an energy range of 67-81.5 MeV.
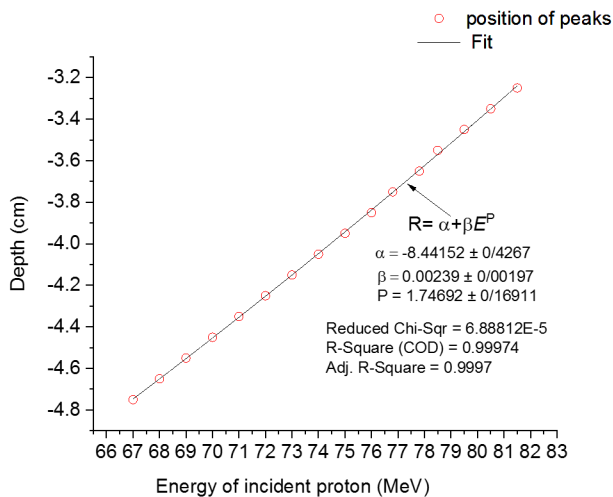

Figure 3. The relationship between the incident proton energy and the position of the Bragg peaks in the gastric tumor.

The values of the factors α, β, and P are approximately -8.44 cm, 2.23×10^{-3} cmMeV^{-1}, and 1.75, respectively. E is measured in MeV and R is measured in cm.

SOBP construction

Figure 4 shows a spread Bragg peak obtained by applying the weighting coefficients calculated with the matrix method to the assumed Bragg peaks. The weighting of each peak indicates its contribution to the formation of the spread Bragg peaks. These weights indicate the radiation time of each beam with a certain energy and are used in the construction of the range modulator. The distance from the distal point of 90% of the maximum dose along the axis of the beam profile as a value for the penetration depth (d'90) is 5.14 cm. The value of the dose reduction from 80% to 20% of the maximum dose as distal dose drop (DDF) is 0.13 cm. The value of the modulation width (90'Mod) as the distance between 90% of the maximum proximal and distal dose is 2.31 cm. The treatment (or target) length is determined by the distance between the single DDF length distal to the proximal 90% dose value of the

SOBP and the double DDF length proximal to the distal 50% dose value of the SOBP.
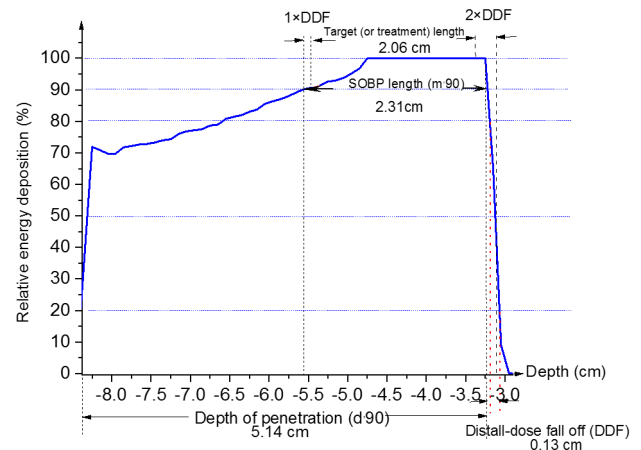
Figure 4. Spread-out Bragg peak resulting from the optimal Bragg peaks and the determining parameters for the characterization of the proton dose distribution of the constructed SOBP.

In figure 5, the proton absorbed dose is plotted by applying weighting coefficients according to the energy of the incident proton beam in the tumor. In this figure, the absorbed dose in the tumor shows an increasing tendency in the mentioned energy range with increasing energy of the incident beam.
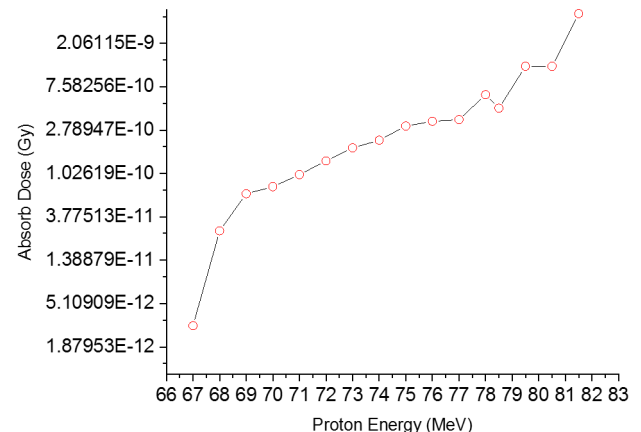
Figure 5. Absorbed dose as a function of proton energy in the gastric tumor.

Distribution of energy deposition in tumor and vital organs

Protons with an energy range of 68-81.5 MeV deposit the most energy to the tumor. The flux and energy of the neutrons and photons produced in the tumor were calculated. Protons with an energy of 75 MeV (the average energy of the proton beams in table 1) produce neutrons with an average energy of 15.7 MeV in the tumor. Of all the neutrons produced, 59.5% have an energy of 1-20 MeV, 34.1% have an energy of 20-68 MeV, and about 6% have less than 1 MeV. The average energy of the photons produced by the interaction of primary protons or secondary particles with the tumor tissue was 4.59 MeV. Most of the photons produced had an energy of 4.44 MeV. They accounted for 7% of all photons produced and

resulted from the reactions of ^{12}C (p, pα) ^{16}O and ^{12}C (p, p') ^{12}C. Figure 6 shows the distribution lines of proton, neutron, photon, and electron energy depositions (sum of electrons and positrons) in depth and laterally due to the SOBP effect. Electrons and positrons are scattered more strongly than other particles due to their charge and low mass. Figure 6b shows the sudden increase in the neutron dose in the tumor area, which leads to the destruction of the tumor. No complications were observed. Figure 6 shows that neutrons, photons, electrons, and positrons account for about 27%, 28%, and 24% of their total energy in the tumor, respectively. In other words, the secondary particles release a significant amount of their energy before they reach and leave the tumor.

Evaluation of proton and secondary particles dose

The doses of secondary particles, such as neutrons, photons, electrons and positrons, were evaluated. The results of the dose evaluation are shown in figure 7. The dose received by organs such as the stomach tissue, body skin, spleen, pancreas, and left kidney was much lower than the dose received by the tumor, but higher than that received by the other body organs. The highest ratio was 10^{-3} for the stomach and 10^{-5} for the skin, and the lowest was 10^{-9} for the brain and thyroid organs. In addition, the neutron dose was higher than that of the other secondary particles. The neutron equivalent dose in the vital organs studied is about 109 times the photon equivalent dose, and the electron absorbed dose is about 34 times the positron absorbed dose.
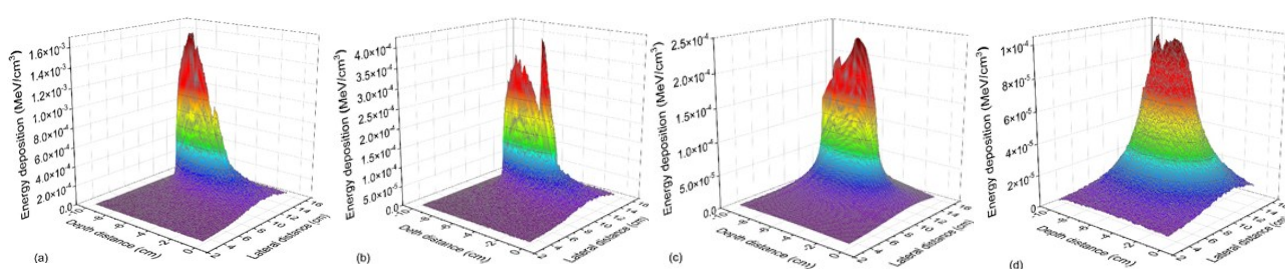

Figure 6. Energy distribution with respect to depth and lateral distance in the tumor and adjacent organs for particles of **(a)** protons, **(b)** neutrons, **(c)** photons and **(d)** electrons.
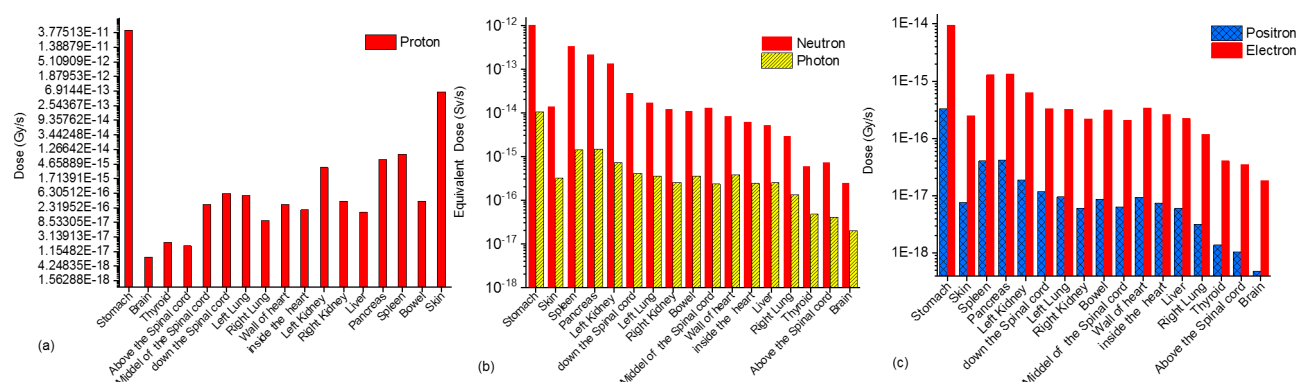

Figure 7. Monte Carlo-simulated doses in vital organs of the body for the particles **(a)** proton, **(b)** neutron and photon and **(c)** electron and positron.

The total absorption dose of electrons and positrons in healthy tissue around the tumor is about 10^{-6} times the proton dose.

Another parameter that clearly shows the efficiency of this treatment method is the calculation of the ratio between the total tumor dose and the dose to other unaffected organs. Figure 8 shows that almost 99.5% of the dose from the whole body phantom was delivered to the tumor, 0.46% to the stomach and less than 0.04% to 11 non-involved organs. This large difference in the dose received by the tumor and other body tissues shows that the healthy tissue was successfully protected from the radiation.

Evaluation of neutron equivalent dose

The H/D values were calculated for the different body tissues. The calculation results are shown in figure 9. According to these values, the highest neutron equivalent dose to the therapeutic absorbed dose (H/D) is found in the stomach, spleen, pancreas and left kidney. The lowest amounts were found in the brain and thyroid gland. Some researchers have confirmed the use of proton therapy for the treatment of gastric cancer [10-15].
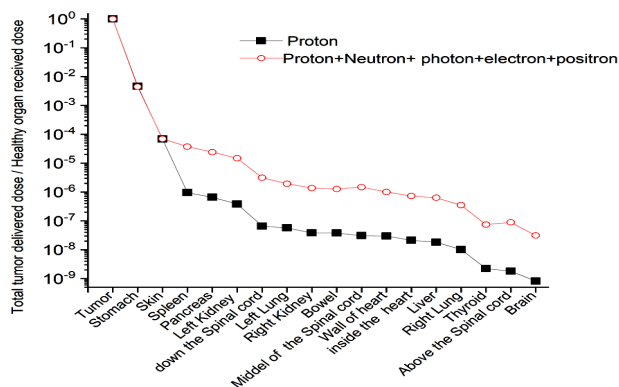
Figure 8. Comparison of the ratio of the total dose delivered to the tumor to the dose received by the healthy organ for proton particles and total particles (primary and secondary).

DISCUSSION

The results in figure 2 show that the height of the Bragg peak decreases by about 5.6% when the neutron energy is increased from 68 to 70 MeV. In a study by Maruf Khani and colleagues, the dose-depth profile in the breast of an ORNL material phantom was calculated for proton energies in the range of 60-70 MeV using the MCNPX code [5]. They show that the height of the Bragg peak decreased by about 6% when the neutron energy was increased from 68 to 70 MeV. The results of this study are comparable to the results of the famous Khani study. This difference is due to the interaction of the different protons with the stomach and breast tissue in these two studies. The results of the secondary particle dose calculations in figure 7b show that the photon equivalent dose is much smaller than the neutron equivalent dose. Marouf Khani et al. have also shown that the photon equivalent dose is about 10^{-2} times the neutron equivalent dose. The comparison of the values of the two studies shows good agreement. This difference in the values may be due to the different proton energies in the two studies. The results of this study are comparable to those of Augusteo *et al.* [18]. They showed that the neutron and photon doses in proton therapy of ocular tumors in a passively scattered proton system, the estimated maximum dose from the generated secondary particles ranged from 10^{-4} to 10^{-2} Gy per treatment Gy. As expected, the secondary particle dose values in figure 7 were lower in the uninvolved organs than the results reported by Augusto.

In a study by Schneider et al., the neutron dose in a water phantom was calculated using the FLUKA Monte Carlo code [19]. They showed that the neutron equivalent dose for a tumor of average size is about 1% of the treatment dose and the dose in the treatment area is negligible for spot scanning proton therapy. In this study, the results in figure 9 show that the neutron dose in the stomach is 0.1% of the treatment dose. This small amount shows the great potential of this treatment method.
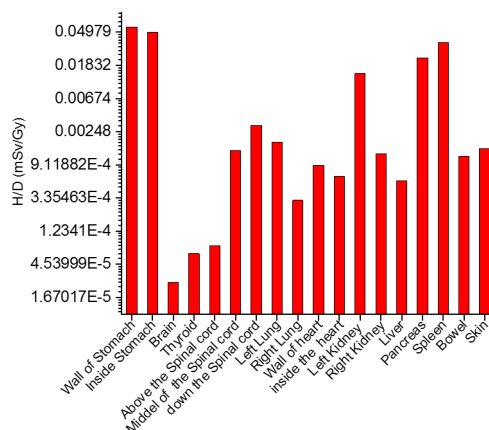
Figure 9. Neutron dose equivalent to the absorbed therapeutic dose (H/D) in different organs of the MIRD-UF phantom.

In a simulation study, Ahmadi *et al.* performed proton dosimetry calculations for the liver tumor of an RNAL- RNAL-MIRD phantom [4]. They showed that the ratio of neutron to proton equivalent dose in organs near the tumor is 10^{-3} for proton therapy with energies of 88-120 MeV, while the overall neutron to proton dose ratio is 10^{-5}. They found that this value is about 10^{-3} for liver tissue and about 10^{-7} for organs far away from the irradiation site, such as the brain. In figure 8, this ratio was reported as 10^{-5} for organs close to the tumor and 10^{-9} for organs far from the irradiation site, such as the brain and thyroid gland. Farah *et al.* also reported that the secondary neutron dose decreases with increasing distance from the treatment field in proton therapy of craniopharyngiomas and ocular melanoma [30]. The results of this study in figures 7b and 9 show that the vital structures such as the untreated gastric tissue and spleen had high levels of secondary neutron dose, which should be taken into account in clinical practice. Additional shielding may be required to protect these structures from external neutrons. In addition, the study showed that the secondary neutron dose decreases with increasing distance from the treatment field. In cases where advanced gastric cancer is not inoperable, clinical studies show that chemotherapy with protons is successful [14]. Studies show that treatment of gastrointestinal cancer with X-rays can cause complications and potentially affect long-term tumor control, even at low doses that spare radiosensitive structures such as the heart, lungs, and intestines. In contrast, studies show that proton beam therapy can improve clinical outcomes [15]. The results obtained in this study confirm the results of previous studies.

CONCLUSION

This study involved irradiating a small gastric tumor in an adult male MIRD-UF phantom with

high-energy protons in proton therapy The SOBP has been determined to deliver a uniform optimal dose to the tumor. Depending on the size of the tumor, the appropriate range for proton energy is between 67 MeV and 81.5 MeV. The results show that the dose of proton particles and other secondary particles in healthy organs during proton therapy in the stomach is less than one percent of the total dose received by the tumor.

Declarations: Ethics approval and consent to participate not applicable.

Consent for publication: Not applicable.

Availability of data and materials: The datasets used and/or analyzed during the current study are available from the corresponding author on reasonable request.

Conflicts of Interest: The authors declare that they have no conflicts of interest.

Author contributions: All authors contributed equally to this study, data curation and analysis and the writing of the manuscript. All authors read and approved the final manuscript.

REFERENCES

1. Schardt D, Elsässer T, Schulz-Ertner D (2010) Heavy-ion tumor therapy Physical and radiobiological benefits. *Reviews of Modern Physics, 82(1): 383.*
2. Paganetti H (2018) Proton therapy physics: CRC press; 2018 Nov 19.
3. Mohan R, Grosshans D (2017) Proton therapy—present and future. *Advanced Drug Delivery Reviews, 109: 26-44.*
4. Ahmadi Ganjeh Z, Eslami-Kalantari M, Mowlavi AA (2019) Dosimetry calculations of involved and noninvolved organs in proton therapy of liver cancer: a simulation study. *Nuclear Science and Techniques, 30(12): 1-7.*
5. Maroufkhani F, Abtahi SMM, Kakavand T (2021) Assessment of secondary particles in breast proton therapy by Monte Carlo simulation code using MCNPX. *Int J Radiat Res, 19(1): 23-29.*
6. Jia SB, Mowlavi AA, Hadizadeh MH, Ebrahimi Loushab M (2014) Impact of range straggling and multiple scattering on proton therapy of brain, using a slab head phantom. *International Journal of Radiation Research, 12(2): 161-167.*
7. Ouar M, Amine Dib AS, Belkaid MN, Belbachir AH (2022) Monte Carlo simulation of a new proton therapy technique using bio-nanoparticles and high energy proton beams. *International Journal of Radiation Research, 20(3): 615-619.*
8. Gillin MT, Sahoo N, Bues M, Ciangaru G, Sawakuchi G, Poenisch F, *et al*. (2010) Commissioning of the discrete spot scanning proton beam delivery system at the University of Texas MD Anderson Cancer Center, Proton Therapy Center, Houston. *Medical Physics, 37(1): 154-163.*
9. Jafari NA, Tajik, M (2024) Reducing secondary particle dose in proton therapy for gastric tumors: a material optimization study. *Journal of Theoretical and Applied Physics, 18(5): 1-11.*
10. Dionisi F, Avery S, Lukens JN, Ding X, Kralik J, Kirk M, *et al*. (2014) Proton therapy in adjuvant treatment of gastric cancer: planning comparison with advanced x-ray therapy and feasibility report. *Acta Oncol, 53(10): 1312-1320.*
11. Ling TC, Kang JI, Slater JD, Yang GY (2012) Proton therapy for gastrointestinal cancers. *Translational Cancer Research, 1(3):150-158.*
12. Mondlane G, Gubanski M, Lind PA, Ureba A, Siegbahn A (2017) Comparison of gastric-cancer radiotherapy performed with volumetric modulated arc therapy or single-field uniform-dose proton therapy. *Acta Oncologica, 56(6): 832-838.*
13. Mondlane G, Ureba ANA, Gubanski M, Lind PA, Siegbahn A (2018) Estimation of Risk of Normal-tissue Toxicity Following Gastric Cancer Radiotherapy with Photon- or Scanned Proton-beams. *Anticancer Research, 38(5): 2619.*
14. Koyama S, Kawanishi N, Fukutomi H, Osuga T, Iijima T, Tsujii H, Kitagawa T(1990) Advanced carcinoma of the stomach treated with definitive proton therapy. *Am J Gastroenterol, 85(4): 443-447.*
15. Shibuya S, Takase Y, Aoyagi H, Orii K, Sharma N, Tsujii H, *et al*. (1991) Definitive proton beam radiation therapy for inoperable gastric cancer: a report of two cases. *Radiat Med, 9(1): 35-40.*
16. Kobeissi JM, Simone CB, Hilal L, Wu AJ, Lin H, Crane CH, Hajj C (2022) Proton Therapy in the Management of Luminal Gastrointestinal Cancers: Esophagus, Stomach, and Anorectum. *Cancers, 14 (12): 2877.*
17. Chuong M, Badiyan SN, Yam M, Li Z, Langen K, Regine W, *et al*. (2018) Pencil beam scanning versus passively scattered proton therapy for unresectable pancreatic cancer. *Journal of Gastrointestinal Oncology, Vol 9, No 4 (August 2018).*
18. Weber DC, Ares C, Lomax AJ, Kurtz JM (2006) Radiation therapy planning with photons and protons for early and advanced breast cancer: an overview. *Radiation Oncology, 1(1): 1-11.*
19. Agosteo S, Birattari C, Caravaggio M, Silari M, Tosi G (1998) Secondary neutron and photon dose in proton therapy. *Radiotherapy and Oncology, 48(3): 293-305.*
20. Schneider U, Agosteo S, Pedroni E, Besserer J (2002) Secondary neutron dose during proton therapy using spot scanning. *International Journal of Radiation Oncology Biology Physics, 53(1): 244-251.*
21. Asadi A, Hosseini SA, Akhavanallaf A, Vosoughi N, Zaidi H (2022) Comparative assessment of passive scattering and active scanning proton therapy techniques using Monte Carlo simulations. *Journal of Instrumentation, 17(09): P09008.*
22. Dent B, Griffin SM (2014) Gastric tumours. *Surgery (Oxford), 32 (11): 608-613.*
23. Im WJ, Kim MG, Ha TK, Kwon SJ (2012) Tumor size as a prognostic factor in gastric cancer patient. *Journal of Gastric Cancer, 12(3): 164-172.*
24. Maughan RL, Chuba P, Porter AT, Ben-Josef E, Lucas DR, Bjarngard BE (1999) Mass energy-absorption coefficients and mass collision stopping powers for electrons in tumors of various histologies. *Medical Physics, 26(3): 472-477.*
25. Hendricks JS, McKinney GW, Fensin ML, James MR, Johns RC, Durkee JW, *et al*. (2008) MCNPX 2.6. 0 Extensions. *Los Alamos National Laboratory, 2008 Apr, 11: 73.*
26. Paganetti H, Niemierko A, Ancukiewicz M, Gerweck LE, Goitein M, Loeffler JS, Suit HD (2002) Relative biological effectiveness (RBE) values for proton beam therapy. *Int J Radiat OncolBiol Phys, 53(2): 407-421.*
27. American Nuclear Society (1977) Working Group ANS. American national standard neutron and gamma-ray flux-to-dose-rate factors: American Nuclear Society.
28. Zheng Y, Newhauser W, Fontenot J, Taddei P, Mohan R (2007) Monte Carlo study of neutron dose equivalent during passive scattering proton therapy. *Phys Med Biol, 52(15): 4481-4496.*
29. OriginPro 2024 (Learning Edition) ed (2024) Nort Hampton, MA, USA.: OriginLab Corporation; 2024.
30. Rezaee L (2018) Design of spread-out Bragg peaks in hadron therapy with oxygen ions. *Reports of Practical Oncology and Radiotherapy, 23(5): 433-441.*
31. Badiyan SN, Hallemeier CL, Lin SH, Hall MD, Chuong MD (2018) Proton beam therapy for gastrointestinal cancers: past, present, and future. *J Gastrointest Oncol, 9(5): 962-971.*